A&A 385, 67–86 (2002)
DOI: 10.1051/0004-6361:20011771

Astronomy & Astrophysics

A new, cleaner colour-magnitude diagram for the metal-rich globular cluster NGC 6528⋆,⋆⋆

Velocity dispersion in the Bulge, age and proper motion of NGC 6528

S. Feltzing[1] and R. A. Johnson[2,⋆⋆⋆]

[1] Lund Observatory, Box 43, 221 00 Lund, Sweden
[2] Institute of Astronomy, Madingley Road, CB3 0HA Cambridge, UK
e-mail: rjohnson@eso.org

Received 20 July 2001 / Accepted 11 December 2001

Abstract. Using two epochs of HST/WFPC2 images of the metal-rich globular cluster NGC 6528 we derive the proper motions of the stars and use them to separate the stars belonging to NGC 6528 from those of the Galactic bulge. The stellar sequences in the resulting colour-magnitude diagram for the cluster are significantly better determined than in previously published data. From comparison of the colour-magnitude diagram with the fiducial line for NGC 6553 from Zoccali et al. (2001) we conclude that the two globular clusters have the same age. Further, using α-enhanced stellar isochrones, NGC 6528 is found to have an age of 11 ± 2 Gyr. This fitting of isochrones also give that the cluster is 7.2 kpc away from us. From the measured velocities both the proper motion of the cluster and the velocity dispersion in the Galactic bulge are found. NGC 6528 is found to have a proper motion relative to the Galactic bulge of $< \mu_l > = 0.006$ and $< \mu_b > = 0.044$ arcsec per century. Using stars with $\sim 14 < V_{555} < 19$ (i.e. the red giant branch and horizontal branch) we find, for the Galactic bulge, $\sigma_l = 0.33 \pm 0.03$ and $\sigma_b = 0.25 \pm 0.02$ arcsec per century. This give $\sigma_l/\sigma_b = 1.32 \pm 0.16$, consistent both with previous proper motion studies of K giants in the Galactic bulge as well as with predictions by models of the kinematics of bulge stars.

Key words. Galaxy: globular clusters: individual: NGC 6528 – Galaxy: bulge – Galaxy: kinematics and dynamics

1. Introduction

NGC 6528 is perhaps *the* most metal-rich globular cluster known and several studies have therefore targeted this cluster, e.g. Ortolani et al. (1992), Ortolani et al. (1995), Richtler et al. (1998), Cohen & Sleeper (1995), Heitch & Richtler (1999), Carretta et al. (2001). It has also been used as a reference in studies of other clusters, e.g. Davidge (2000). We summarize important literature measurements of NGC 6528 in Table 1.

NGC 6528 is at $(l, b) = (1.14, -4.12)$, i.e. in the plane of the Galactic disk and towards the Galactic bulge. The first effect of this is that it is heavily reddened by foreground dust, Ortolani et al. (1992), Richtler et al. (1998), Heitsch & Richtler (1999). Most recent distance estimates put the cluster within less than 1 kpc from the Galactic centre (e.g. Richtler et al. 1998 and references therein). The close proximity to bulge stars further complicates the interpretation of the colour-magnitude diagram. Since the bulge stars and the cluster stars have roughly the same distance modulus they are superimposed in the colour-magnitude diagram. This effect has been noted to be particularly pronounced in the red giant branch (Richtler et al. 1998).

In a pre-study we noted in particular that the colour-magnitude diagram of the globular cluster NGC 6528 closely resembled that of NGC 5927 *if* the latter was superimposed on the colour-magnitude diagram of Baade's window (for a set of representative colour-magnitude diagrams see Feltzing & Gilmore 2000). This is consistent with the cluster being virtually inside the Galactic bulge and thus having a large contribution of bulge stars in its colour-magnitude diagram. Moreover, if the cluster is as

Send offprint requests to: S. Feltzing,
e-mail: sofia@astro.lu.se

⋆ Based on observations with the NASA/ESA Hubble Space Telescope, obtained at the Space Telescope Science Institute, which is operated by the Association of Universities for Research in Astronomy, Inc. under NASA contract No. NAS5-26555.

⋆⋆ Tables A1, A2 and A3 are only available in electronic form at the CDS via anonymous ftp to cdsarc.u-strasbg.fr (130.79.128.5) or via
http://cdsweb.u-strasbg.fr/cgi-bin/qcat?J/A+A/385/67

⋆⋆⋆ *Present adress*: ESO, Alonso de Cordova, Vitacura 3107, Santiago, Chile

Table 1. Data for NGC 6528 compiled from the literature.

	Value	Ref.	Comment
Core radius	$0\farcm09$	Harris (1996)	
Distance	7.5 kpc	Ortolani et al. (1992)	
$\Delta(m-M)$	16.4	Zinn (1980)	19.1 kpc
	14.35	Ferraro et al. (1999)	
	15.15 ± 0.24	Heitsch & Richtler (1999)	isochrone fitting
[Fe/H]	+0.01	Zinn (1980)	
	+0.29	Bica & Patoriza (1983)	
	+0.12	Zinn & West (1984)	
	−0.23	Armandroff & Zinn (1988)	Integrated spectra IR Ca II
	high, sim to NGC 6553	Ortolani et al. (1992)	
	−0.23	Origlia et al. (1997)	IR abs. at 1.6 μm
	$+0.07 \pm 0.1$?	Carretta et al. (2001)	
[M/H]	+0.1/−0.4	Richtler et al. (1998)	Trippico isochrone/Bertelli isochrone
	−0.31	Ferraro et al. (1999)	
	0.00	Heitsch & Richtler (1999)	
Z	$Z_\odot$	Bruzual et al. (1997)	
Age	14 Gyr	Ortolani et al. (1992)	metallicity comparable to solar
	12 ± 2 Gyr	Bruzual et al. (1997)	
$E(B-V)$	0.56	Zinn (1980)	
	0.55	Ortolani et al. (1992)	NGC 6553 as reference and $\Delta(m-M)_V = 14.39$
	0.62	Bruzual et al. (1997)	
	0.62	Ferraro et al. (1999)	
$E(V-I)$	0.8/0.6	Richtler et al. (1998)	Trippico isochrone/Bertelli isochrone
	0.46 ± 0.03	Heitsch & Richtler (1999)	isochrone fitting

metal-rich as indicated in previous studies (and now confirmed by Carretta et al. 2001) then the red-giant branch as well as both the turn-off and the horizontal branch of the bulge and globular cluster will appear at virtually the same magnitudes and colours. The bulge stars will be more spread out in the colour-magnitude diagram than those in the cluster, due to the large range of metallicities and ages present in the bulge (e.g. McWilliam & Rich 1994; Feltzing & Gilmore 2000). Thus the only way to obtain a clean colour-magnitude diagram for the cluster is to obtain proper motions of the cluster stars relative to the bulge stars and separate the two populations using their proper motions.

This conclusion prompted us to apply for HST time to obtain a second epoch of observations of NGC 6528 with WFPC2 in order to derive the relative proper motion of the cluster as compared to that of the Galactic bulge.

We report here on the results from this proper motion study. The article is organized as follows; Sect. 2 presents the data, derivation of photometry and proper motions are discussed in Sects. 3 and 4, Sects. 5 and 6 contain an extensive discussion of mean proper motions and velocity dispersions for NGC 6528 relative to the Galactic bulge as well as the velocity dispersion in the bulge itself, in Sect. 7 we use the proper motion information to obtain a clean colour-magnitude diagram for NGC 6528, Sect. 8 contains a discussion of the age for the cluster, and finally Sect. 9 provides a brief discussion and conclusions.

Table 2. NGC 6528 HST/WFPC2 observations used in this study.

GO	Filter	Exp. time (s)	
5436	$F555\,W$	2×100	1×5
5436	$F814\,W$	2×50	1×14
8696	$F555\,W$	8×100	1×5
8696	$F814\,W$	2×50	

2. The data

The data consist of two sets of observations, one from the HST archive and observed in 1994 (GO 5436) and the other our new data for the same field (GO 8696, PI Feltzing). We detail the number of exposures in each filter and epoch as well as integration times in Table 2. The first data set was taken on the 27 February 1994 and the new one (GO 8696) on the 1 April 2000. This gives a time span of 6.093 years between the two set of observations.

The first epoch of observations provided a long and a short set of exposures in $F555\,W$ and $F814\,W$ with the

cluster centre on WF3. Our new observations were observed with the same WFPC2 orientation, but with four times as long total exposure time in $F555\,W$. The increased exposure times enable us to reliably detect all the possible stellar sources in the first epoch data.

A new pair of $F814\,W$ images were also taken in order to improve the accuracy of the $F814\,W$ magnitudes. Finally, one short exposure in $F555\,W$ was also obtained in order to find the proper motions of the brightest stars in the field which are saturated in the longest exposures.

The images for each filter/epoch combination were combined using the DRIZZLE and CRREJ tasks in the STSDAS environment within IRAF[1]. Drizzling removes the WFPC2 geometric distortion from the images.

For the first epoch data we combined the $F555\,W$ and $F814\,W$ images into one single image to obtain as deep an image as possible for object centering.

3. Stellar photometry

Stellar photometry was done inside the DIGIPHOT.DAOPHOT package in IRAF. In particular we found the stars using DAOFIND on the deep, new $F555\,W$ images, then aperture and psf-photometry were obtained using PHOT and ALLSTAR on the same images. For the aperture photometry we used an aperture of 2 pixels. For the psf-photometry psfs variable over the chips, constructed from the images themselves, were used and the output statistics, i.e. χ and sharpness, were used to weed out non-stellar sources.

This created a list of stars that were then used for obtaining aperture photometry from the new $F814\,W$ images, which together with the $F555\,W$ data gave a first colour-magnitude diagram. The positions of the stars making up the colour-magnitude diagram provided our source list of objects to find proper motions for.

For the images with short exposures we performed aperture photometry on the first epoch images for each filter and then merged the $F555\,W$ and $F814\,W$ data into a colour-magnitude diagram. Keeping only stars detected in both $F555\,W$ and $F814\,W$ this provided a master list for bright objects to find the proper motions for in the short exposures.

The final colour-magnitude diagrams are all based on the aperture photometry.

3.1. Calibration

We obtained instrumental ($-2.5\log$(counts/s),) magnitudes from both the old, short and new, long exposure data. These magnitudes were corrected to the HST/WFPC2 magnitude system, and merged to form a final single photometry set as described below.

[1] IRAF is distributed by National Optical Astronomy Observatories, operated by the Association of Universities for Research in Astronomy, Inc., under contract with the National Science Foundation, USA.

Table 3. Values of constants found for aperture correction in each image, see Sect. 3.1.

	$F555\,W$		$F814\,W$	
	a	b	a	b
Short				
WF2	0.17	1.70e-4	0.21	1.78e-4
WF3	0.21	1.47e-4	0.23	1.90e-4
WF4	0.27	2.21e-4	0.23	1.59e-4
Long				
WF2	0.24	5.42e-5	0.27	4.35e-5
WF3	0.24	2.16e-4	0.28	1.84e-4
WF4	0.24	1.17e-4	0.23	1.07e-4

The final stellar magnitudes within the HST/WFPC2 system i.e. V_{555} and I_{814}, were obtained by applying a number of corrections to the instrumental magnitudes, essentially following Holtzmann et al. (1995b).

The photometry was obtained from drizzled images. The drizzling procedure removes the geometric distortion from the images, therefore no geometric distortion correction was required for the photometry.

Aperture corrections to a 0.5 arcsec aperture were obtained from our own images. These corrections were allowed to vary with distance from the centre of the chip i.e. correction $= a + b\times$distance The values of the constants a and b are given in Table 3. For the WF4 long data there were not enough stars to obtain both a and b from our data. In this case we used the value of b from Gonzaga et al. (1999) and only fit the value of a from our data. Corrections for the charge transfer (in)efficiency (CTE) were applied. The short data were obtained before the WFPC2 cool-down on 23/4/1994. The CTE problem is worse for the pre-cool-down data, but the corrections are not well modeled. For these data the CTE problem was corrected by assuming that the star counts lost were a linear function of the y-position on the chip, with stars at the top of the chip losing the maximum 10% (Holtzmann 1995b). For our new long data we used the equations in Whitmore et al. (1999) to correct for CTE.

The zero-points used to transform to HST/WFPC2 magnitudes are from Baggett et al. (1997).

3.2. Merging long and short photometry

To make the final colour magnitude diagrams we have merged the photometry from the long and short exposures. We compared the magnitudes of the same stars from the short and long exposure data, and found no evidence for any offsets. Further, we found that the long exposure data were saturated for $V_{555} < 16.8$ and $I_{814} < 15$.

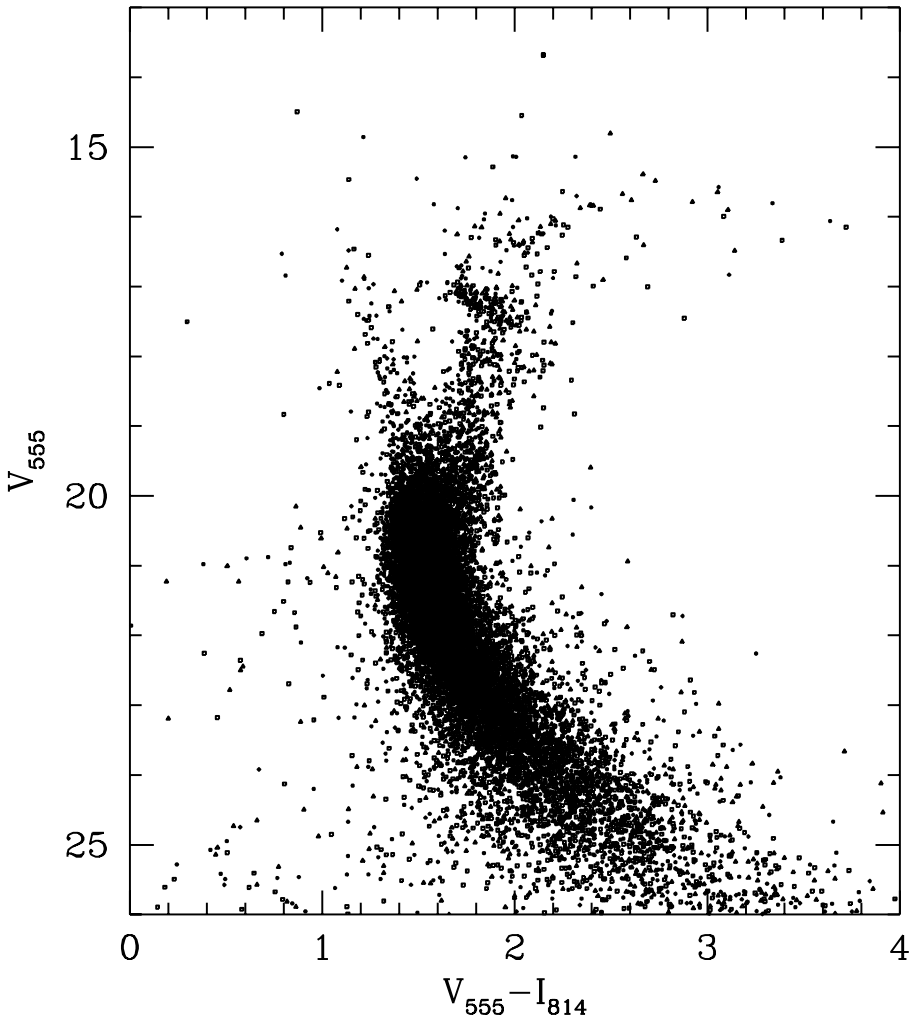

Fig. 1. Colour-magnitude diagram for all three WF. All stars measured in both the new and old images and which satisfied the cuts imposed in χ and sharpness variables (see Sect. 3) on the individual WFs are included. Stars with fitting errors are excluded.

The two sets of long and short photometry were then merged according to the following rules

- if the star has both long and short photometry then use long if $V_{555} > 16.8$ and $I_{814} > 15$, otherwise use short;
- if the star just has short photometry then use it if $V_{555} \leq 16.8$ or $I_{814} \leq 15$;
- if the star just has long photometry then use it if $V_{555} > 16.8$ and $I_{814} > 15$.

Our final colour-magnitude diagram is shown in Fig. 1. This includes all stars selected according to our selection criteria for χ and sharpness. We also require the stars to all have good positions according to the photometric routines in DAOPHOT. No corrections for differential reddening have been applied.

4. Proper motions

The heart of this investigation is to use the measured proper motions to separate out the bulge and cluster stars. Our chosen method to find the proper motion for each star consists of the following steps:

1. find the transformation, x- and y-shifts as well as rotation (small in our case), between the two epochs of observations using a small number of bright stars;
2. transform the positions on the new images (the deep drizzled $F555W$ images in our case) to the reference frame of the old images;
3. re-center the transformed positions on the old image (in our case we used the deep image combined from both filters for this);
4. inspect the x- and y-shifts found in the re-centering, select only stars that have small shifts relative to the centre of the distribution of shifts;
5. using only those stars selected in the previous item find a new, improved transformation between the epochs;
6. apply the new solution and re-center the stars on the old image;
7. if deemed necessary iterate.

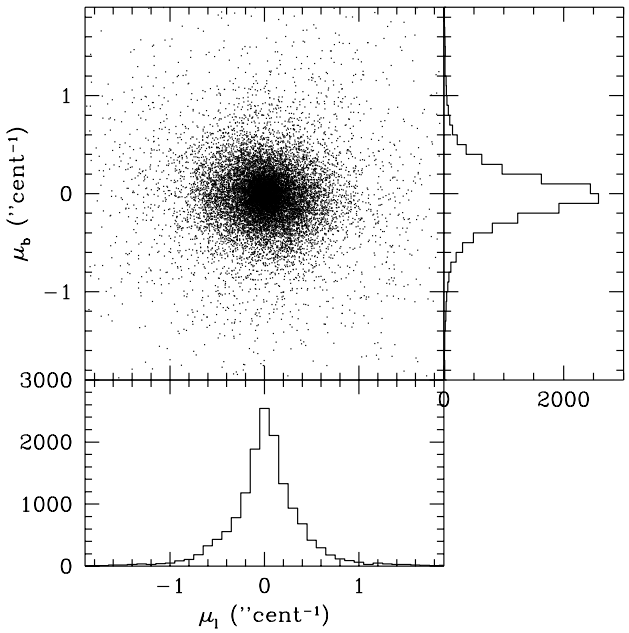

Fig. 2. Stellar proper motions and the resulting histograms for μ_l and μ_b. The proper motions are measured in arcsec per century.

We only needed to iterate a few times to find our solutions. Since the WF chips in the WFPC2 over time slowly drift relative to each other, Fruchter & Mutchler (1998), the transformations between the new and the old reference frames have to be found separately for each WF-chip.

For the short exposures we first applied the transformation found from the deep images. However, since it appears that the new short exposure is not perfectly aligned with the new deep images we iterated the solution for the transformation once.

5. Measuring proper motions and velocity dispersions

The shifts obtained (in pixels) for the individual WFs were transformed to a common grid, i.e. the Galactic coordinates, as well as to arcsec per century ($''$ cent^{-1}). In Fig. 2 these proper motions are plotted together with the histograms for the proper motions in l and b. The full data set for stars brighter than $V_{555} = 19$ (proper motions, positions, and magnitudes) is given in the Tables in Appendix A.

In an ideal scenario, where the globular cluster has an appreciable motion in relation to the bulge stellar population, the bulge and cluster stars will form two distinct distributions in the proper motion diagram. See for example the recent results by Zoccali et al. (2001) for NGC 6553, King et al. (1998) for NGC 6739 and Bedin et al. (2001) for M 4, or those for NGC 6712 by Cudworth (1988). The bulge stars have a larger velocity dispersion than the cluster stars, and hence a larger scatter in the proper motion diagram.

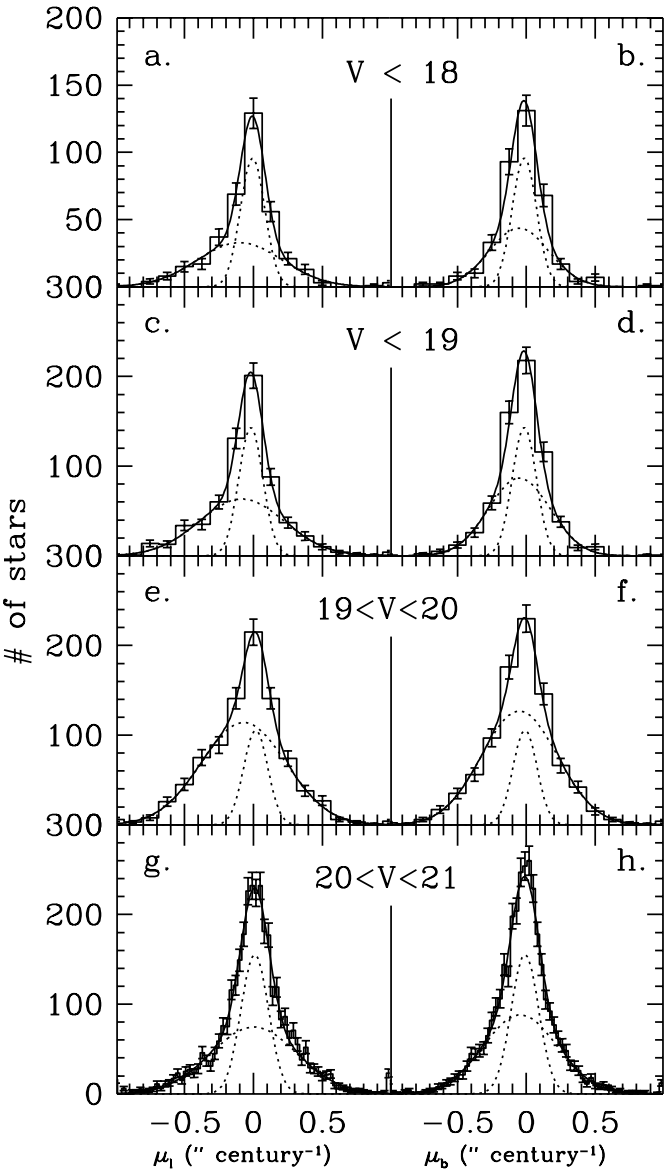

Fig. 3. Histograms for the l and b proper motions (μ_l, μ_b) for different magnitude ranges (as indicated). For each histogram Poissonian errorbars are drawn as well as the fitted Gaussians. The dotted lines show the two Gaussians needed to fit the data and the full line the final combined distribution. The fitted parameters are given in Table 4. Proper motions are measured in arcsec per century.

In our case Fig. 2 shows that the motion of the globular cluster in relation to the Galactic bulge is very small. This is as expected since the heliocentric radial velocity relative to the local standard of rest for NGC 6528 is high (184.9 ± 3.8 km s^{-1}, Harris 1996; $\simeq$210 km s^{-1}, Carretta et al. 2001), which suggests that NGC 6528 is on a mostly radial orbit away from us. However, we note that the histograms for the velocities in the l and b coordinates have broad wings. In fact when we tried to fit our histograms with Gaussian distributions it became clear that a single Gaussian distribution could not fit the observed distributions and two Gaussians were needed.

Table 4. Gaussian fits to proper motion distributions in Fig. 3. An error of 0. indicates that that particular parameter was kept fixed during the fitting procedure. We give the amplitude, the center ($<\mu>$), and the σ for two Gaussians (shown with dotted lines in Fig. 3). Both are in arcsec per century. The first fours rows give the results for the l-coordinate and the last for for the b-coordinate.

Galactic l		Field			Cluster	
mag. range	Amp_1	$<\mu_1>$	σ_1	Amp_2	$<\mu_2>$	σ_2
		(arcsec century^{-1})			(arcsec century $^{-1}$)	
$V<18$	32.783 ± 5.990	-0.097 ± 0.027	0.305 ± 0.025	95.539 ± 11.934	-0.005 ± 0.010	0.088 ± 0.011
$V<19$	63.362 ± 7.231	-0.084 ± 0.017	0.306 ± 0.012	142.831 ± 14.992	-0.018 ± 0.009	0.088 ± 0.009
$19 \leq V < 20$	114.083 ± 9.793	-0.072 ± 0.013	0.305 ± 0.009	105.318 ± 16.496	0.017 ± 0.014	0.087 ± 0.015
$20 \leq V < 21$	74.461 ± 4.957	0.004 ± 0.008	0.309 ± 0.007	155.211 ± 7.769	0.010 ± 0.005	0.099 ± 0.006
Galactic b		Field			Cluster	
$V<18$	43.627 ± 5.509	-0.052 ± 0.018	0.214 ± 0.014	$95.539 \pm 0.$	-0.014 ± 0.012	$0.088 \pm 0.$
$V<19$	86.681 ± 7.088	-0.051 ± 0.013	0.221 ± 0.009	$142.831 \pm 0.$	-0.015 ± 0.010	$0.088 \pm 0.$
$19 \leq V < 20$	126.907 ± 6.433	-0.050 ± 0.011	0.273 ± 0.007	$105.318 \pm 0.$	-0.009 ± 0.015	$0.088 \pm 0.$
$20 \leq V < 21$	87.990 ± 3.073	-0.044 ± 0.007	0.265 ± 0.004	$155.211 \pm 0.$	-0.010 ± 0.005	$0.099 \pm 0.$

To separate the bulge and cluster stars using the measured proper motions, we divide the stars into different magnitude ranges and find the best fitting Gaussians, as shown in Fig. 3. We found that two Gaussians were required to fit the data well, indicating that, as expected, we have two stellar populations with different velocity dispersions. Based on previous measurements of bulge and cluster velocity dispersions, we associate the narrow Gaussian with NGC 6528 and the broad Gaussian with the bulge stars.

We found that the μ_l-diagram was easily fit by two Gaussians by our routine, however μ_b proved more difficult. In fact the fitting routine found one badly fitting broad Gaussian for the data in Fig. 3. However we expect the cluster stars to have the same velocity dispersion and amplitude in l and b and so we fixed the parameters for the narrower Gaussian, which represents the cluster stars, from the fitting of the μ_l-distribution. In particular we fixed the height and the width but left the position free to be fitted. The second Gaussian had all three parameters (width, height and position) free for fitting. The results for all the fitted Gaussians are given in Table 4.

We find that all four μ_l-distributions are fit by two Gaussians, one narrow and with a $\sigma_l \approx 0.08$ arcsec per century, and one broader with $\sigma_l \approx 0.30$ arcsec per century. The centers of these Gaussians vary with magnitude range, see Table 4. For the broad Gaussian in μ_l the three brightest magnitude ranges agree very well within the calculated errors while for the last bin the center has moved from ~ -0.07 to 0 arcsec per century. For the narrow Gaussian the centers for the two brightest magnitudes agree within the errors, as do those for the two faintest magnitudes.

For μ_b we fixed the fwhm and height for the narrow Gaussian before fitting (see discussion above). Thus by definition $\sigma_b = \sigma_l$ and amplitude$_b$ = amplitude$_l$ for each magnitude range for the narrow Gaussian. For the broad Gaussian we find a σ_b around 0.21. Unlike the μ_l distribution, the fitted centres for the broad and narrow Gaussians in μ_b remain consistent within the errors for all the magnitude bins. The centers for the two Gaussians are found to be -0.05 ± 0.01 and -0.012 ± 0.012 arcsec per century.

The different behaviour of the centers of the μ_l and μ_b histograms with magnitude suggests the presence of a stellar component in addition to the bulge and cluster stars that is adding an additional proper motion component to μ_l. One possibility for this component is disk stars, which may be the main component of the blue plume seen in the colour-magnitude diagram in Fig. 1. We therefore investigate below whether we see any difference in Gaussians fit separately to blue and red samples.

In Figs. 4 and 5 we divide the two bright magnitude samples, $V_{555} \leq 19$ and $19 < V_{555} < 20$ into red and blue stars and fit Gaussians to them in the same way as before. The fitted parameters are given in Table 5.

For the blue stars ($V_{555} - I_{814} < 1.6$) in the brightest sample, i.e. $V_{555} < 19$, it proved impossible to fit two Gaussians both for μ_l and μ_b. Since there are few stars in these two histograms we have carefully checked that the chosen binning did not effect the final result. The results are given in Table 5.

The red samples, on the other hand, show a very strong central peak and broad wings which means that two Gaussians are needed to achieve a good fit. As before we first fitted the μ_l distribution and then fixed the σ and amplitude for the narrow Gaussian when fitting the μ_b distribution. It is interesting to find that indeed the

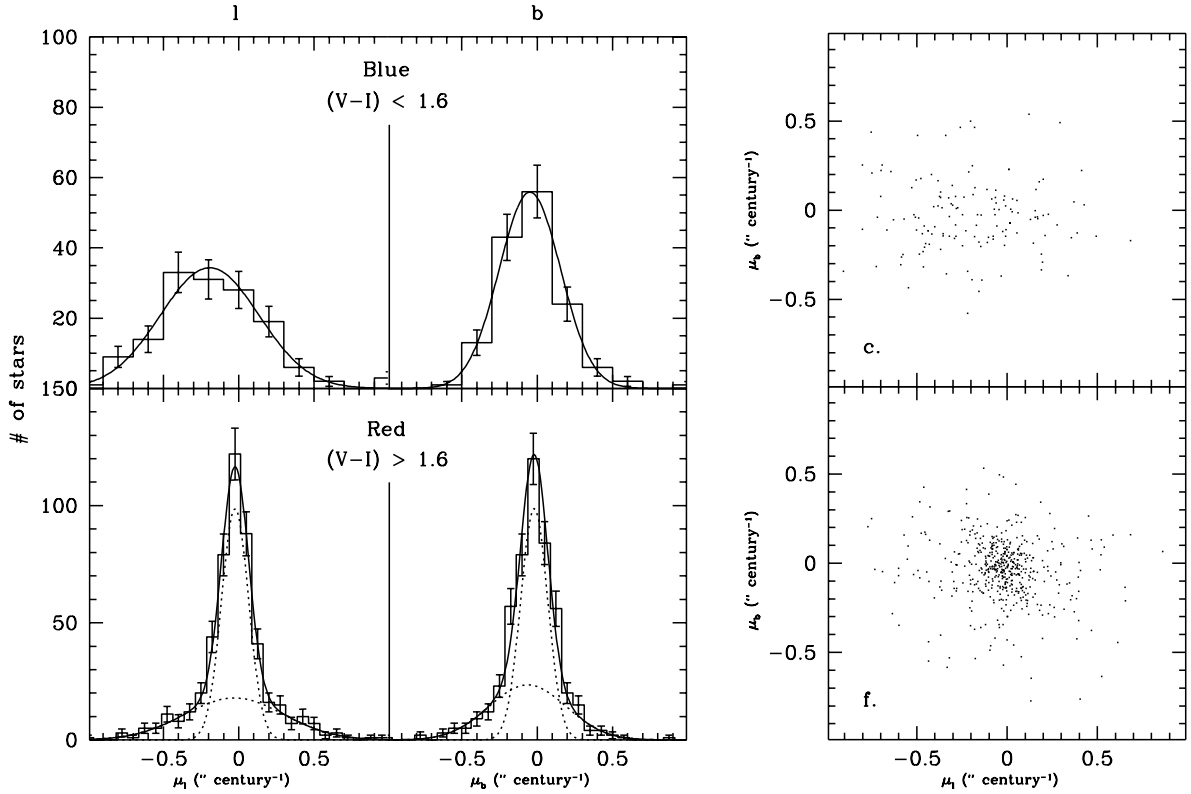

Fig. 4. Histograms for the b and l proper motions (μ_l, μ_b) for blue, $V-I<1.6$, and red, $V-I>1.6$, stars all with $V_{555}\leq 19$. For each histogram Possonian errorbars are drawn as well as the fitted Gaussians. For the blue samples only one Gaussian is fitted, while for the red two Gaussians are necessary to fit the data (see text for discussion). The fitted parameters are given in Table 5. Proper motions are measured in arcsec per century.

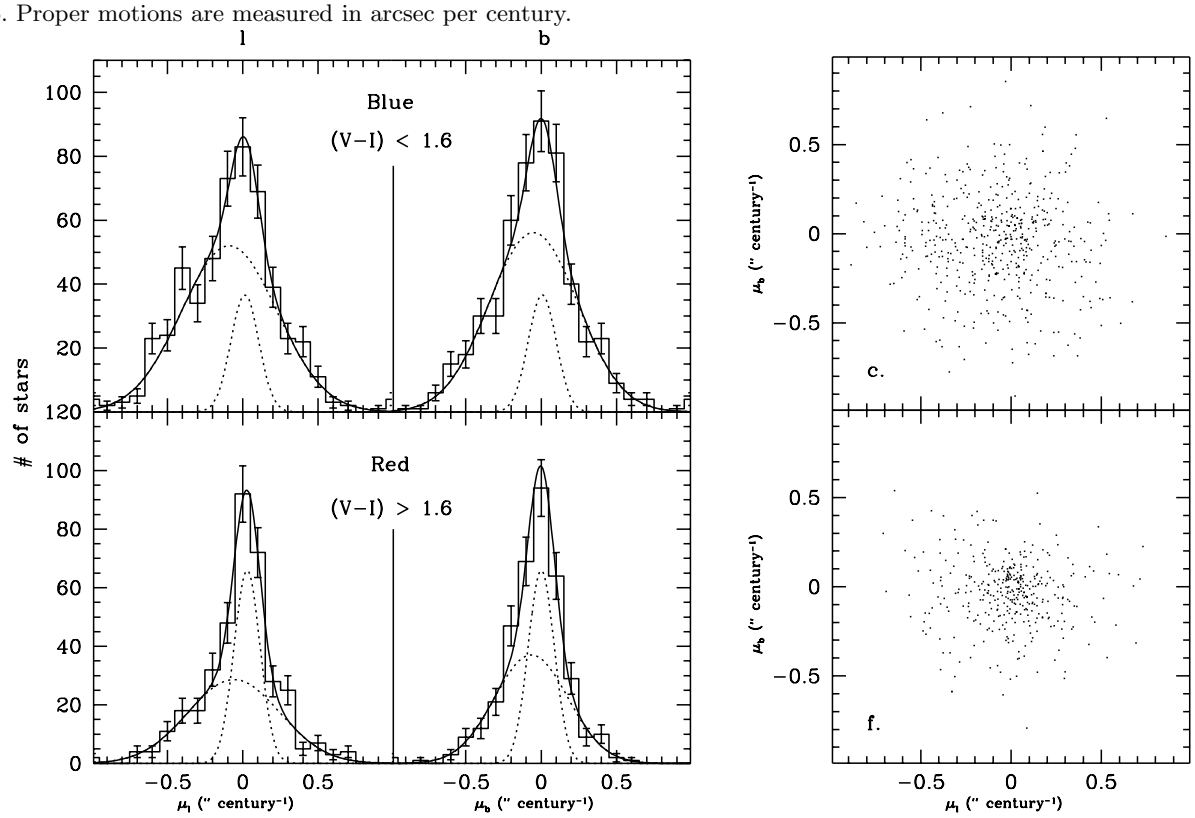

Fig. 5. Histograms for the b and l proper motions (μ_l, μ_b) for blue, $V-I<1.6$, and red, $V-I>1.6$, stars all with $19<V_{555}<20$. For each histogram Possonian errorbars are drawn as well as the fitted Gaussians. For the blue samples only one Gaussian is fitted, while for the red two Gaussians are necessary to fit the data (see text for discussion). The fitted parameters are given in Table 5. Proper motions are measured in arcsec per century.

Table 5. Gaussian fits to proper motion distribution in Figs. 4 and 5. An error of 0. indicates that that particular parameter was kept fixed during the fitting procedure. We give the amplitude, the center ($< \mu >$), and the σ for two Gaussians (shown with dotted lines in the figures). Both are in arcsec per century.

Galactic l		Field			Cluster		
Mag. range	Colour	Amp_1	$< \mu_1 >$ (arcsec century^{-1})	σ_1	Amp_2	$< \mu_2 >$ (arcsec century^{-1})	σ_2
$V < 19$	$V-I < 1.6$	34.332 ± 3.485	-0.193 ± 0.028	0.324 ± 0.020			
$V < 19$	$V-I > 1.6$	17.912 ± 3.496	-0.030 ± 0.026	0.327 ± 0.027	98.707 ± 8.215	-0.024 ± 0.007	0.089 ± 0.007
$19 < V < 20$	$V-I < 1.6$	51.985 ± 6.185	-0.090 ± 0.018	0.314 ± 0.014	36.609 ± 9.312	0.014 ± 0.024	0.092 ± 0.028
$19 < V < 20$	$V-I > 1.6$	28.649 ± 5.302	-0.059 ± 0.025	0.302 ± 0.025	65.822 ± 9.429	0.029 ± 0.012	0.085 ± 0.013
Galactic b		Field			Cluster		
$V < 19$	$V-I < 1.6$	55.828 ± 5.611	-0.048 ± 0.017	0.202 ± 0.011			
$V < 19$	$V-I > 1.6$	23.495 ± 3.135	-0.063 ± 0.021	0.254 ± 0.017	$98.707 \pm 0.$	-0.019 ± 0.008	$0.089 \pm 0.$
$19 < V < 20$	$V-I < 1.6$	56.149 ± 3.678	-0.051 ± 0.015	0.291 ± 0.010	$36.609 \pm 0.$	0.007 ± 0.025	$0.092 \pm 0.$
$19 < V < 20$	$V-I > 1.6$	37.056 ± 3.878	-0.066 ± 0.018	0.241 ± 0.013	$65.822 \pm 0.$	0.001 ± 0.013	$0.085 \pm 0.$

narrow Gaussian has a $\sigma = 0.08$ arcsec per century, exactly the same as found when the full colour-range was investigated.

We also investigate the distributions for the magnitude range 19 to 20, Fig. 5. Here, again, we see a rather broad dominating dispersion in the blue while the red is dominated by the narrow distribution, even if not as prominently as in the case of the brightest stars. The main change between the fit parameters for the sample split by colour and for the whole sample, is that in l the center for the blue sample is significantly different from the red sample, and both the blue and red centers are different to that found when the whole sample is fitted. We suggest that this is due to some of the bright blue stars being from a third stellar population, namely the Galactic disk, which has an additional velocity component in l. We note that the stars identified with the Galactic disk have a mean proper motion in l that is negative relative to that of the Galactic bulge. Disk dwarf stars at the magnitudes observed here should be within a kpc or less from us (see e.g. Sadler et al. 1996). If the rotation curve of the disk (which is not well sampled for these type of objects) differs somewhat from pure differential rotation then this can explain our measured proper motions for stars at these distances.

6. The proper motion of NGC 6528 and the velocity dispersion in the Bulge

The measured proper motions can be used to find the mean proper motion of NGC 6528 relative to the Galactic bulge, and the bulge and cluster velocity dispersions.

As discussed above, it appears that the bright blue stars contain a Galactic disk component. Therefore we use the bright ($V < 19$), red ($V - I > 1.6$) sample to get the final values for cluster and bulge velocity dispersion and proper motion given in Table 6. This then gives us a cluster proper motion relative to the bulge of $< \mu_l > = 0.006$ and $< \mu_b > = 0.044$ arcsec/century. The velocity dispersion for the cluster, 0.08 arcsec per century, translates to 24−30 km s^{-1} for the upper and lower distance limits to NGC 6528 of 6.5 kpc and 8 kpc (Richtler et al. 1998). (The distance found by Ortolani et al. (1992) is 7.5 kpc.)

Globular clusters in the Galaxy have measured velocity dispersions that range from a few km s^{-1} to ∼20 km s^{-1}, see Pryor & Meylan (1993) and Dubath et al. (1997). In M 31 at least two globular clusters have measured velocity dispersions >20 km s^{-1}, Dubath & Grillmar (1997). Zoccali et al. (2001) found $\sigma = 28$ km s^{-1} for NGC 6553. This result is very similar to ours. Since most globular clusters in the Galaxy have significantly lower velocity dispersion they concluded that their measured $\sigma_{\rm cluster}$ was dominated by measurement error. This is most likely also the case for NGC 6528.

Assuming the cluster velocity dispersion in NGC 6528 is dominated by errors, we deconvolve this from the measured velocity dispersion for the bulge to find the true bulge velocity dispersion. Using the data for the red sample (Table 5 with $V_{555} < 19$) we get $\sigma_{l\ \rm bulge} = 0.33 \pm 0.03$ and $\sigma_{b\ \rm bulge} = 0.25 \pm 0.02$ arcsec per century. These numbers are in good agreement with the results for bulge giants found by Spaenhauer et al. (1992), $\sigma_{l\ \rm bulge} = 0.32 \pm 0.01$ and $\sigma_{b\ \rm bulge} = 0.28 \pm 0.01$ arcsec per century for their full sample of 429 stars.

These numbers give a $\sigma_l/\sigma_b = 1.32 \pm 0.16$, which is identical, within the error estimates, to the 1.33 predicted for the coordinates of NGC 6528 by the model of kinematics in the Galactic bulge in Zhao (1996).

In their study of NGC 6553 Zoccali et al. (2001) derived $\sigma_{l\ \rm bulge} = 0.26 \pm 0.03$ and $\sigma_{b\ \rm bulge} = 0.21 \pm 0.02$ arcsec per century giving $\sigma_l/\sigma_b = 1.24 \pm 0.17$. These values are lower than found here, however, NGC 6553 is situated further out from the Galactic centre than NGC 6528 and we should thus expect $\sigma_{l\ \rm bulge}$ to be a factor ∼0.86 lower than for the coordinates of NGC 6528, see Zhao (1996) Table 6. $\sigma_{b\ \rm bulge}$ should remain roughly the same. Specifically the model of Zhao (1996) predicts a $\sigma_l/\sigma_b = 1.32$ at $l = 1$, $b = -4$ and $\sigma_l/\sigma_b = 1.09$ at $l = 5$, $b = -3$, which is consistent, within the errors,

Table 6. Final values for velocity dispersion and mean proper motion. An error of 0. indicates that that particular parameter was kept fixed during the fitting procedure. All values are in arcsec century^{-1}.

	σ_l	σ_b	$< \mu_l >$	$< \mu_b >$
Bulge	0.327 ± 0.027	0.254 ± 0.017	-0.030 ± 0.026	-0.063 ± 0.021
Cluster	0.089 ± 0.007	$0.089 \pm 0.$	-0.024 ± 0.007	-0.019 ± 0.008

to the values found here and in Zoccali et al. (2001) for the bulge stars observed in the fields of NGC 6528 and NGC 6553 (which are situated close to the coordinates for which Zhao's model makes its predictions).

We may thus conclude that these two new studies of the proper motions of Galactic bulge stars confirm the predictions by models of the kinematics in the Galactic bulge. To our knowledge the current work and that of Zoccali et al. (2001) are the first studies to address the velocity dispersion, measured by proper motions, of bulge stars below the horizontal branch.

We can use the measured proper motions ($< \mu_l > = \sim +0.006$ and $< \mu_b > = \sim +0.044$ arcsec per century) of the cluster relative to the Galactic bulge along with a radial velocity of 210 km s^{-1} (Carretta et al. 2001), cluster distance of 7.5 kpc (Ortolani et al. 1992), solar peculiar velocity relative to the local standard of rest of $(u_\odot,\ v_\odot,\ w_\odot) = (10,\ 5.25,\ 7.17)$ km s^{-1} (Dehnen & Binney 1998) and the rotational velocity of the local standard of rest of 239 km s^{-1} (Arp 1986) to calculate the absolute space velocity components of NGC 6528. These are $(\Pi,\ \Theta,\ W) = (-220,\ 17.4,\ 16.1)$ km s^{-1} (Π points radially outwards from the Galactic centre towards the cluster, Θ is oriented in the direction of Galactic rotation, and W points towards the north Galactic pole, and we have made the simplifying assumption that the cluster is at $(l, b) = (0, 0)$).

In an attempt to estimate the internal errors on the derived velocities we varied the proper motions for the cluster according to the errors derived when fitting the histograms and we find that the Π velocity is unaffected by the errors while Θ varies between $\sim$8 and $\sim$27 km s^{-1} and W between $\sim$8 and $\sim$23 km s^{-1}. These should represent maximal internal errors in our analysis and thus we can conclude that the velocities derived are fairly robust.

7. The colour-magnitude diagram and the proper motions

Our new colour-magnitude diagram is presented in Fig. 1. It contains all the photometry from both long and short exposures, as described in Sect. 3.

Clearly visible is the stubby red horizontal branch. The red giant bump, roughly 0.5 mags below the horizontal branch is less easily isolated but appears to be present. To the left a "plume" of field stars and/or blue stragglers in the cluster stretches up from the turn-off region. The turn-off region itself is identifiable but appears confused. The exact position of the sub-giant branch is difficult to establish since it is contaminated with field stars from both the disk and bulge. The red-giant branch rises rather vertically but then appear to turn-over heavily to the red. The red-giant branch itself is very wide. This could be an indication of differential reddening and/or large contamination from bulge stars roughly at the same distance modulus as NGC 6528 but with a spread in both age and metallicity.

The question now is whether the broad red giant branch and the fuzzy sub-giant branch are mainly the result of differential reddening, see e.g. Ortolani et al. (1992), or are primarily caused by contamination of the colour-magnitude diagram by bulge stars (Richtler et al. 1998).

7.1. Applying the proper motions to isolate the cluster

The idea is now to use the proper motions to separate the cluster and bulge stars. There are at least two interesting points here. The first is to know how well we can "decontaminate" the red giant branch of NGC 6528 from bulge stars. Secondly, we want to find out how many of the stars in the "blue" plume above the turn-off realistically belong to the bulge, to the cluster, or to the foreground disk. Also here we would like to know how well we can clean the turn-off region from contaminating stars. The quality of the turn-off region is a major limitation in the case of NGC 6528 for determining a reliable relative or absolute age.

We use our Gaussian fits to the different regions of the colour-magnitude diagram to estimate the proper motion cuts which maximize the number of cluster stars relative to the number of bulge stars, whilst still allowing enough cluster stars to make a good cluster colour-magnitude diagram. Using different proper motion cuts in different regions of the colour-magnitude diagram will affect the relative numbers of cluster stars in each region but this does not matter for comparison of the observed colour-magnitude diagram with other globular clusters and with isochrones, where all we use is the position of the cluster stars in the colour-magnitude diagram and not their number density.

In Fig. 6, we show the effect of various different proper motion cuts imposed on the WF2 colour-magnitude diagram. We have previously found that the cluster has a $\sigma = 0.09$ arcsec per century. In the following we will use this σ when defining the cuts to clean the colour-magnitude diagram. In a we show the full colour-magnitude diagram for WF2. Plot c and d then shows the resulting colour-magnitude diagram when a cut of $\sqrt{\mu_l^2 + \mu_b^2} < 0.09$ and

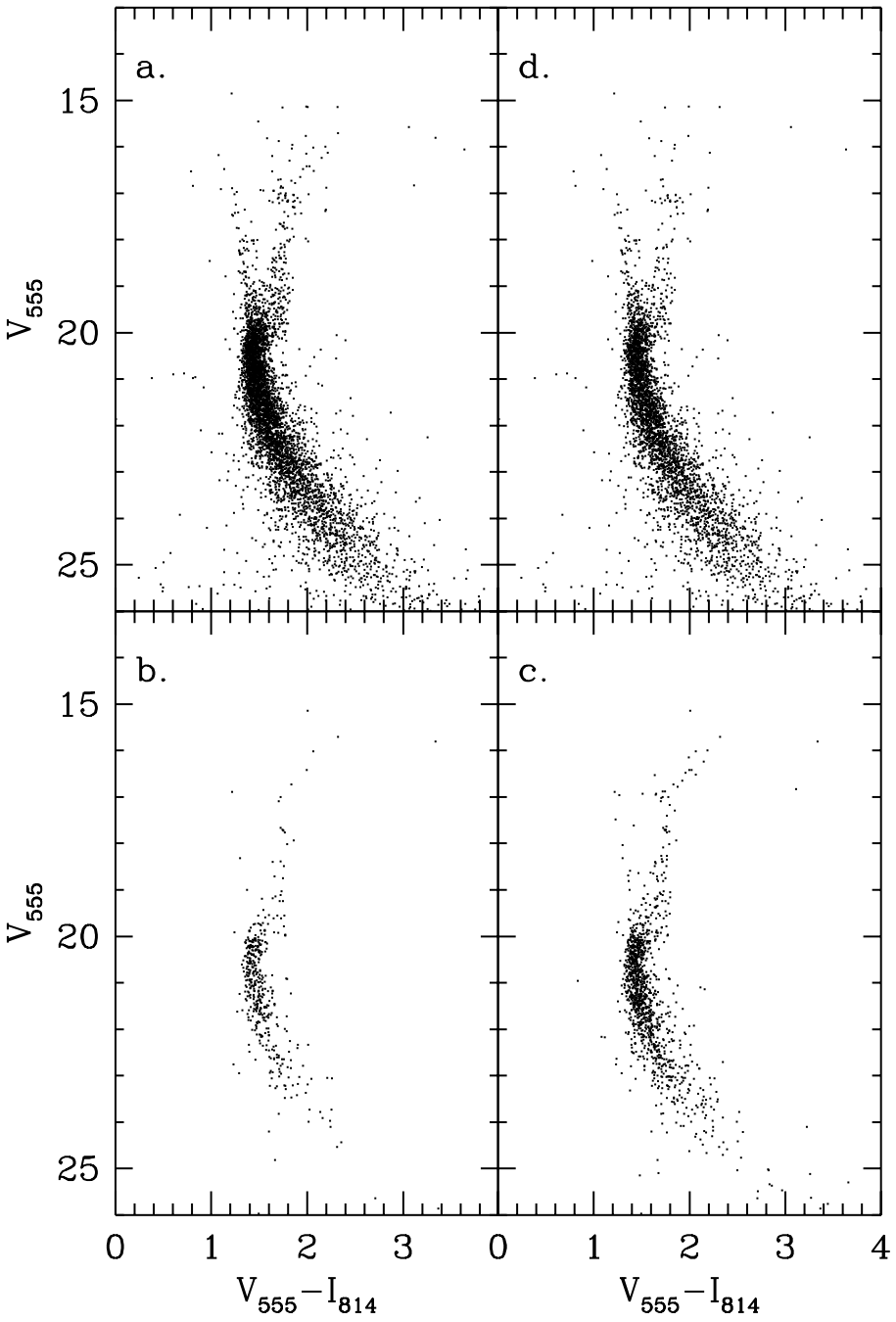

Fig. 6. Illustration for WF2 of the effect on the colour-magnitude diagram from different cuts in $\sqrt{\mu_l^2+\mu_b^2}$. All stars are measured in both the new and old images and satisfy the cuts imposed in χ and sharpness variables (see Sect. 3). Stars with fitting errors are excluded. **a)** all stars, **d)** stars with $\sqrt{\mu_l^2+\mu_b^2} > 0.18$, i.e. the rejected (mainly bulge) stars, **b)** stars with $\sqrt{\mu_l^2+\mu_b^2} < 0.09$, and **c)** $\sqrt{\mu_l^2+\mu_b^2} < 0.18$

$\sqrt{\mu_l^2+\mu_b^2} < 0.18$, have been applied respectively. For the most conservative cut the turn-off region becomes clean, although the sub-giant branch remains somewhat confused. The number of stars in the giant branches, however, becomes almost too small for quantitative work. Moreover, as seen in Fig. 4, for the brighter magnitudes the red part of the colour-magnitude diagram, i.e. the giant branches, is dominated by cluster stars and a more generous cut can be allowed when cleaning the colour-magnitude diagram. This is shown in c. Here though the turn-off region again becomes too confused for good work.

Our cleaned colour-magnitude diagram, Fig. 7, is finally obtained by imposing the following cuts; $\sqrt{\mu_l^2+\mu_b^2} < 0.18$, for star with $V_{555} < 19$ and $\sqrt{\mu_l^2+\mu_b^2} < 0.09$ for the fainter stars.

In Fig. 6b, finally, we show the stars that have $\sqrt{\mu_l^2+\mu_b^2} > 0.18$. These are mainly bulge stars. Compare also the various histograms.

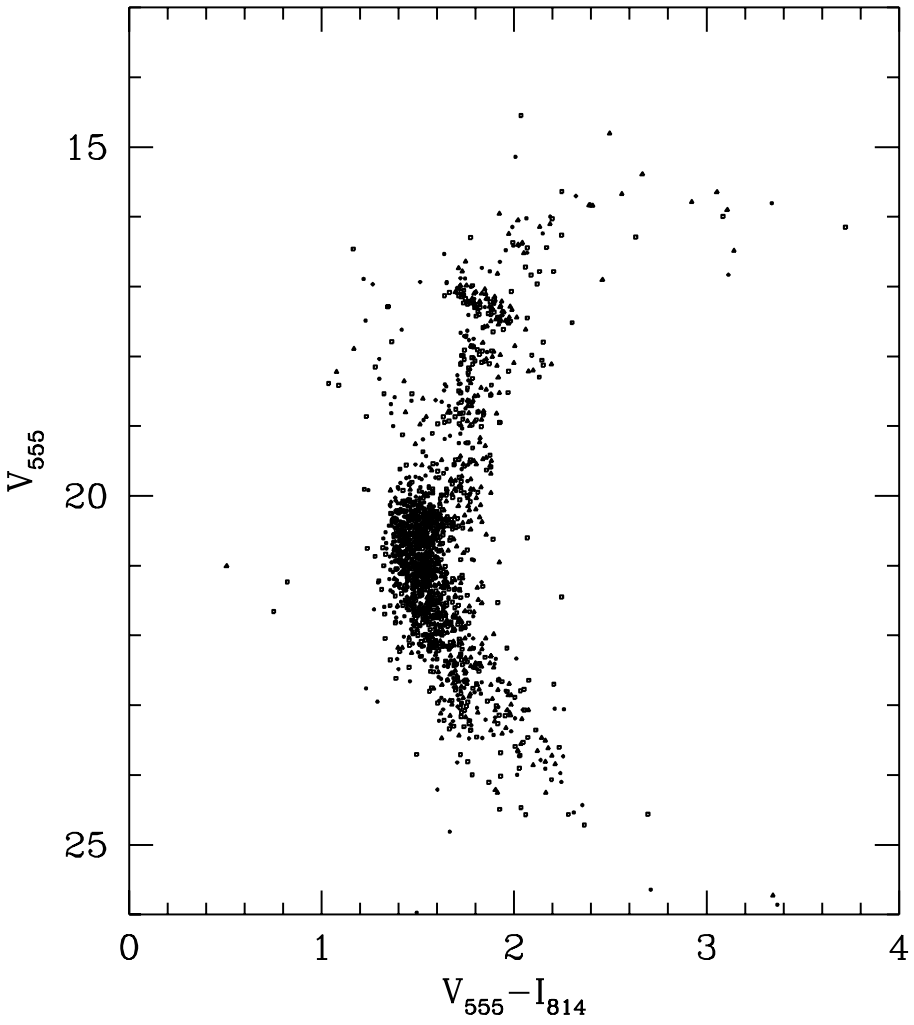

Fig. 7. Colour-magnitude diagram from WF234 for the stars with $\sqrt{\mu_l^2+\mu_b^2} < 0.09$ for $V_{555} \geq 19$ and $\sqrt{\mu_l^2+\mu_b^2} < 0.18$ for the brighter stars.

Figure 8 shows the colour-magnitude diagram for the stars that have $\sqrt{\mu_l^2+\mu_b^2} > 0.18$, i.e. mainly bulge stars. This diagram is now based on all three WFs. This colour-magnitude diagram has large spreads everywhere. Particularly noteworthy is the plume of stars that emanates from the turn-off region as well as the extremely fuzzy appearance of the regions around the horizontal branches, indeed almost a lack of horizontal branch. This colour-magnitude diagram should be compared to that of Baade's window, see e.g. Feltzing & Gilmore (2000) and Fig. 2 in Holtzman et al. (1998). We note also that the red giant stars show a branch that is turning over significantly.

For stars brighter then $V_{555} = 19$ Fig. 9 shows how the stars, included and excluded, from the colour-magnitude diagram are distributed on the sky. The first panel shows the stars that have the highest probability to belong to the globular cluster, i.e. small proper motions and redwards of 1.6 in colour. The second shows the stars that are most likely to belong to either the bulge or to be foreground disks stars. These plots give further support for our definition of cuts in proper motion when defining the stars that belong to the cluster. Figure 9a show a fairly concentrated structure, which tapers of at a certain radius. Note that the detection of stars in the very centre is limited because here we are only using the short exposures since the long were too crowded for good positions. Figure 9b on the other hand shows a much more even distribution of stars.

7.2. Differential reddening towards NGC 6528

We quantify how much of the apparent spread in the colour-magnitude diagram in Fig. 7 is due to differential reddening by fitting the "straightest" portion of the red giant branch for each chip using a linear least squares fit. This is shown in Fig. 10. In the final panel the fits for the three different WFs are compared. From this it is clear that, in the *mean*, the reddening differs between the three chips such that WF2 has the smallest reddening and WF3 has the largest. These reddening estimates are obtained only for stars that most likely belong to the cluster, i.e. the same cuts are imposed in all the following plots as we did in Fig. 7.

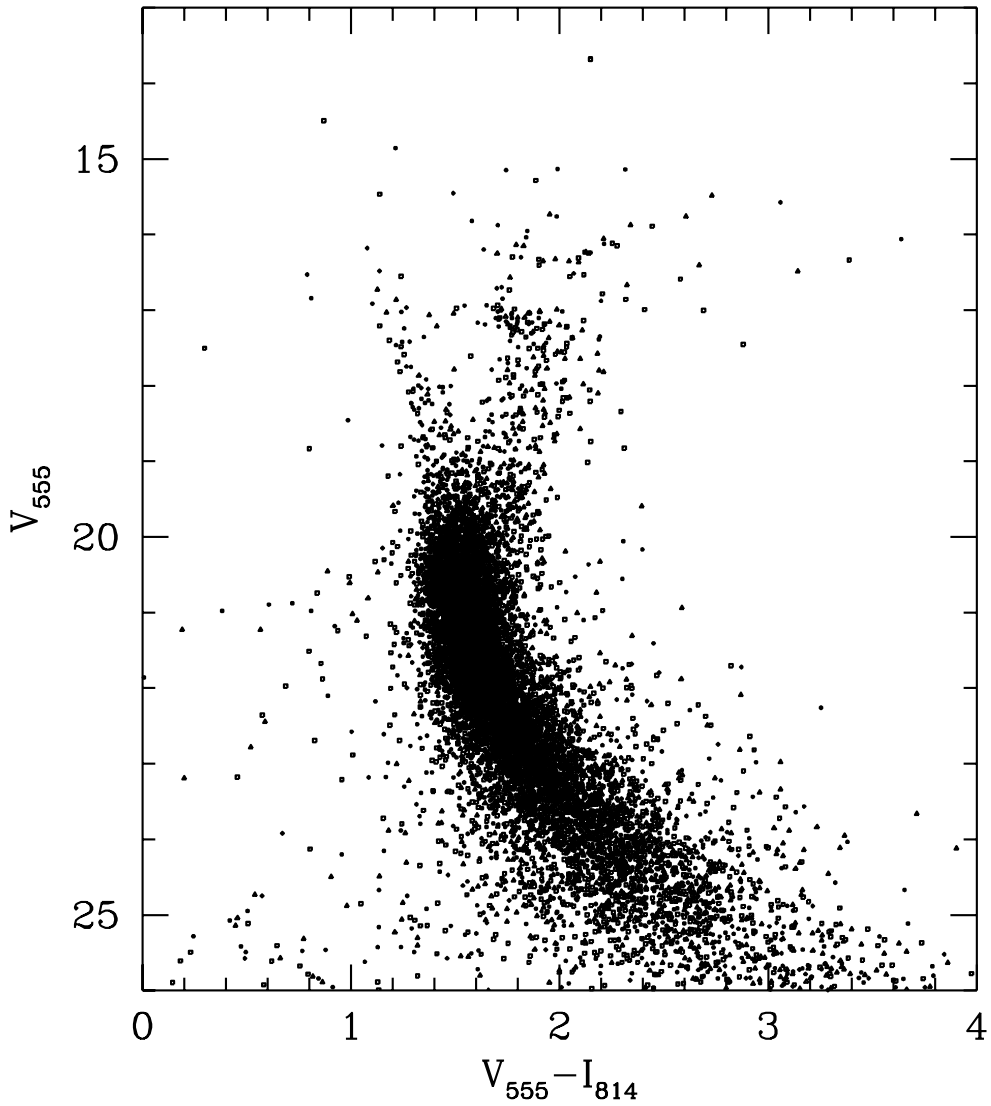

Fig. 8. Colour-magnitude diagram from WF234 for stars rejected as mainly bulge stars due to their proper motions are included, i.e. $\sqrt{\mu_l^2 + \mu_b^2} > 0.18$.

We also consider below whether differential reddening is significant within each chip.

WF2 The giant branch in the colour-magnitude diagram derived from WF2 is quite tight and well defined. We take this as an indication that the differential reddening over this chip is small and that no correction for differential reddening within the chip is needed.

WF3 We divide the image into four sections and construct the colour-magnitude diagrams for each of them in Fig. 11. Again stars on the cleanest portion of the giant branch are selected and fitted with a straight line. First we fit it to all the stars on the chip (full line). Then for each quadrant of the image (dashed lines). From this it is clear, although the number statistics are low, that quadrant 1, 3, and 4 all are close to the mean value, while quadrant 2 has a larger reddening than the rest. As the scatter around the fitted line for that part of the image is small we do not further divide the image into smaller sections but will correct stars in quadrant 2 according to this shift, see Table 7. First we found the shift in $V_{555} - I_{814}$. Then we used Holtzman et al. (1995b) Table 12 to find the corresponding ΔV_{555} that should be applied to remove the colour difference.

Table 7. Differential reddening corrections for the quadrants of WF3 to the mean reddening of WF2. In each case the values indicate how much the stars were moved in order for their fiducial line for the red giant branch to coincide with that of the bluest one within the WF. We used the extinction laws and values in Holtzman et al. (1995b).

Quadrant	$\Delta(V_{555} - I_{814})$	ΔV_{555}
1, 3, 4	−0.106	−0.273
2	−0.151	−0.388

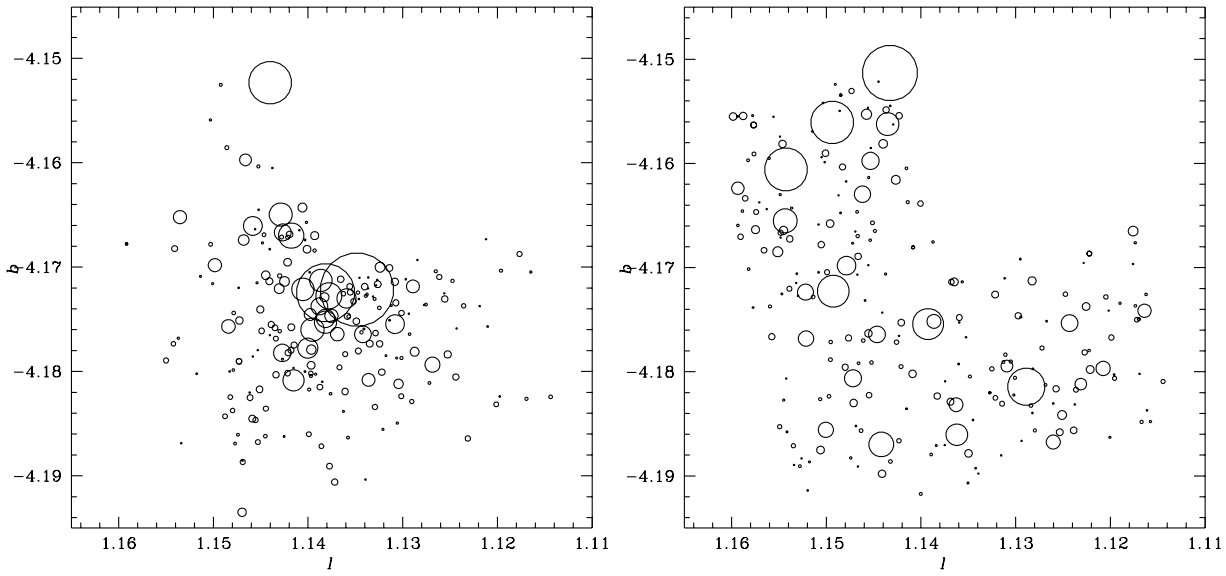

Fig. 9. Positions on the sky for **a)** stars with $V_{555} < 19$, $\sqrt{\mu_l^2 + \mu_b^2} < 0.09$, and $V_{555} - I_{814} > 1.6$. This should be predominantly cluster stars. In **b)** stars with $V_{555} < 19$, $\sqrt{\mu_l^2 + \mu_b^2} \geq 0.18$ and for all colours. This selection should primarily give us bulge and foreground disk stars. The sizes of the symbols code the magnitude of the stars.

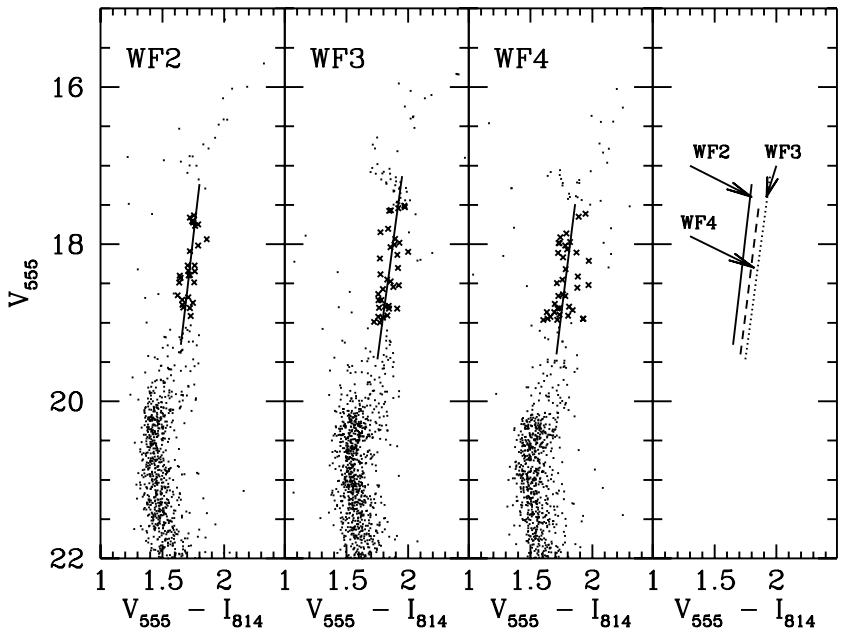

Fig. 10. Colour-magnitude diagrams for WF234 as indicated. Stars used to provide a linear-least square fit to the red giant branch are shown as ×. The fits are indicated by full lines for the individual chips and in the last panel with full (WF2), dotted (WF3) and, dashed (WF4) lines.

Figure 12 shows the WF3 colour-magnitude diagram corrected for differential reddening.

WF4 The colour-magnitude diagram for this chip has the largest spread on the giant branch. Figure 13 shows the result for the four subsections.

For quadrant 3 on the chip nothing can be said since the number statistics is too low. Quadrant 2 appears to be well lined up with the mean value for the chip and quadrant 4 has somewhat larger reddening than quadrant 2. The colour-magnitude diagram for the first quadrant, however, has a remaining large scatter and we further subdivide this quadrant into four sub-quadrants, Fig. 14. This shows that the largest scatter emanates from sub-quadrant 3 and that the three remaining sub-quadrants have a reddening that is less than the mean reddening for the first quadrant. However, because of the complexity found for the differential reddening we will omit WF4 from further discussions.

Our full final colour-magnitude diagram, using data from WF2 and WF3 corrected for differential reddening, is shown in Fig. 15.

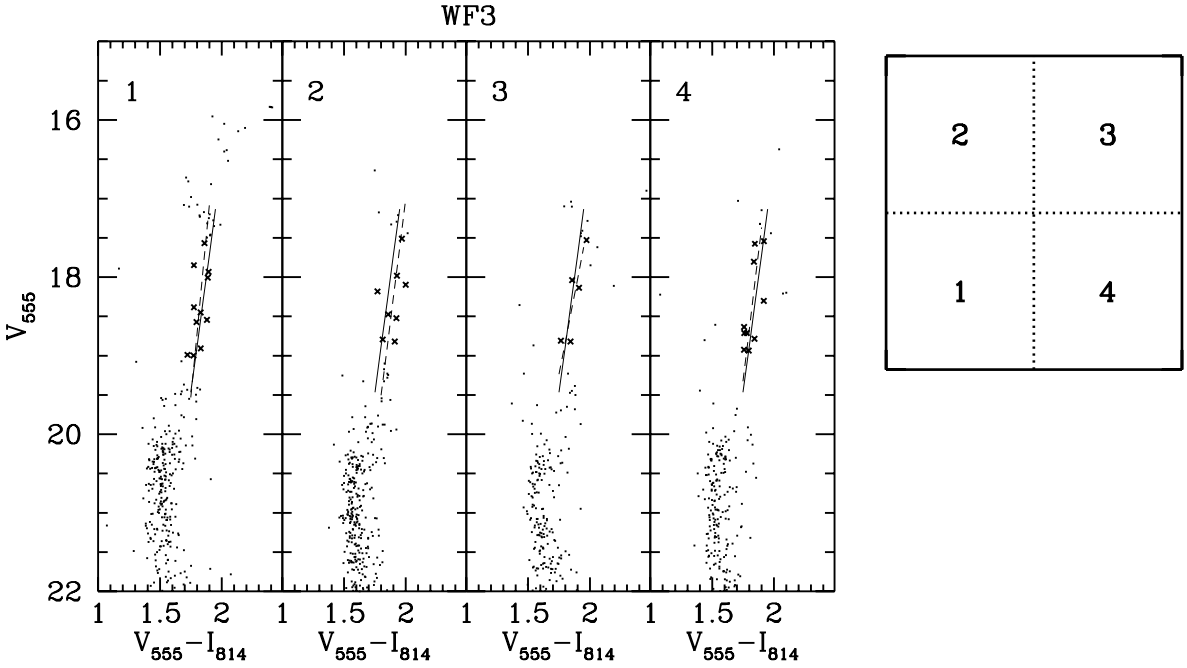

Fig. 11. Colour-magnitude diagrams for the four quadrants of WF3. The division of the chip and labeling of the resulting colour-magnitude diagrams are shown to the right.

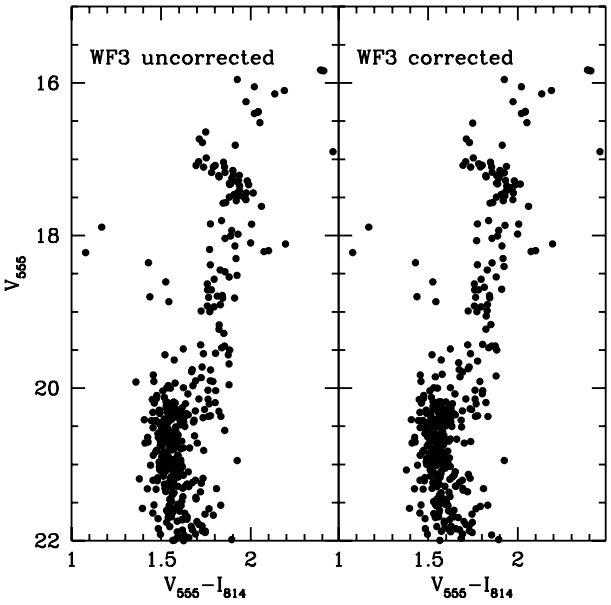

Fig. 12. The effect achieved by correcting the second quadrant of WF3 for differential reddening with respect to the other three quadrants (see Fig. 11). A reddening of $E(V_{555} - I_{814}) = 0.0447$ was applied.

We observe that the red giant branch is more pronounced when the reddening corrections have been applied (see also Richtler et al. 1998). The red subgiant branch bump, even though it is not a strong feature in our colour-magnitude diagram, appears more rounded and well-defined. Heitch & Richter (1999) used the lumpiness of this feature to assess the quality of their differential dereddening. Thus we take the improvement in our corrected colour-magnitude diagram of this feature as an indication that the differential reddening that has been applied is the correct one.

7.3. The tilt of the HB and the curved asymptotic giant branch

For a long time it has been known that one of the characteristics of metal-rich globular clusters in comparison with the metal-poor clusters is the presence of a strongly curved red asymptotic giant branch in the optical. This effect is caused by the extra line blanketing provided by the numerous molecular lines, e.g. TiO, present in the spectra of cool metal-rich giant stars. The complexity of such spectra is illustrated by e.g. Fig. 2 in Ortolani et al. (1991). In Ortolani et al. (1992) the optical colour-magnitude diagram for NGC 6528 shows just this curved structure. Richtler et al. (1998) were able to define a sample of NGC 6528 stars extending all the way out to $V - I \sim 6.5$, showing an exceptionally curved red giant branch and asymptotic giant branch (AGB) which after $V - I \sim 4$ progressively deviates from the predictions from stellar evolutionary tracks (see their Fig. 7).

Figure 15 shows the full extent of our AGB. There are a few red stars that are fainter than the majority of the AGB. These stars could be members of the bulge, but could also, obviously belong to the cluster and be in a region which has a larger differential reddening which is on such a small scale that our previous investigation could not detect it.

An upper envelope for the AGB has been found, but since we here are only using material from two WFPC2 chips the field of view is small we are content with saying

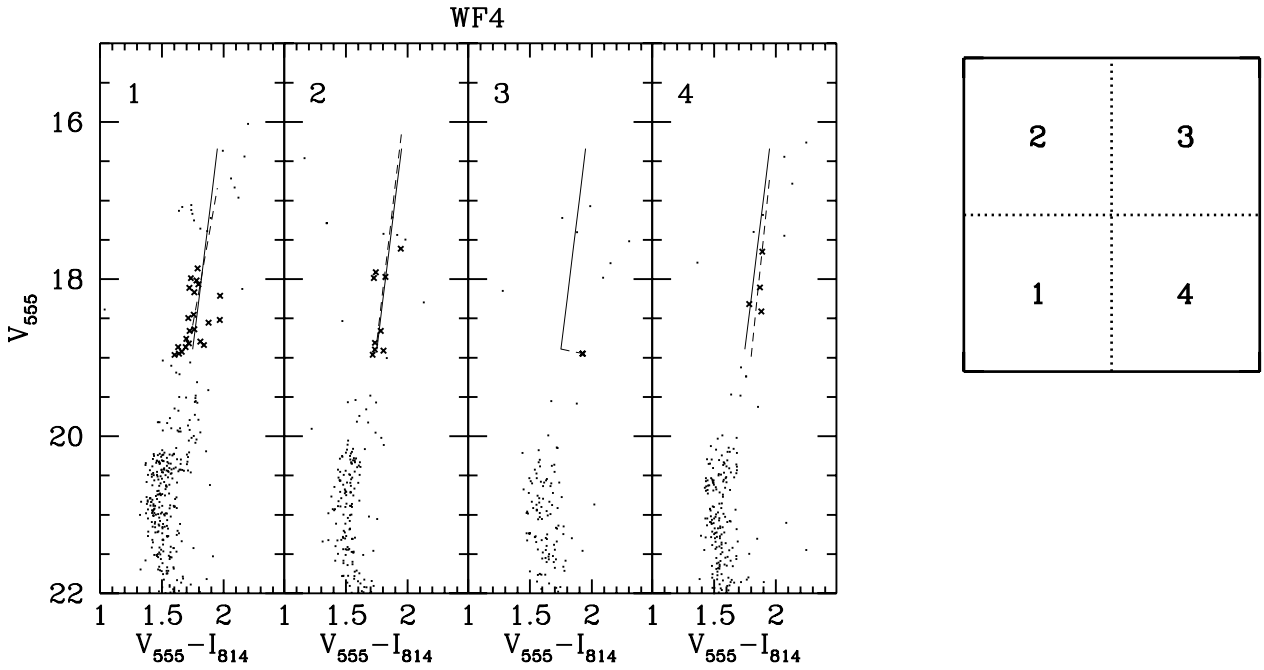

Fig. 13. Colour-magnitude diagrams for the four quadrant of the WF3 image. The division of the chip and labeling of the resulting colour-magnitude diagrams are shown to the right.

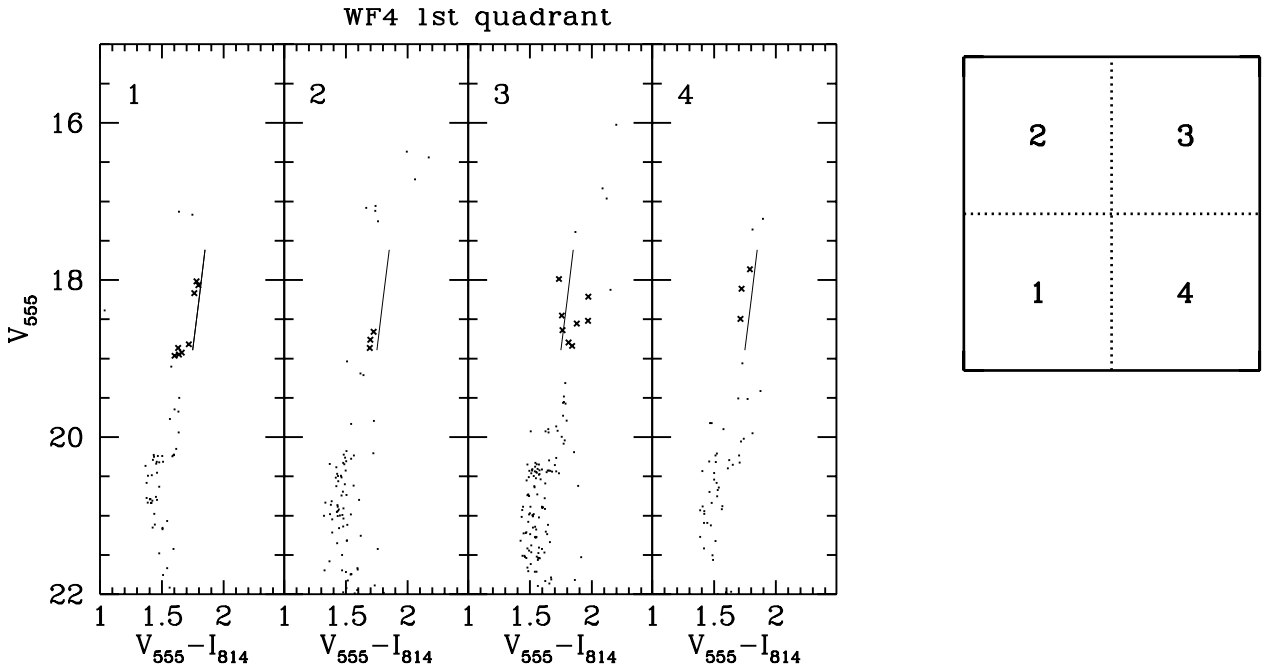

Fig. 14. Colour-magnitude diagrams for the four sub-quadrants of the first quadrant of WF4 image. The division of the chip and labeling of the resulting colour-magnitude diagrams are shown to the right.

that our results agree well with those of Richtler et al. (1998) for the upper envelope, see their Fig. 7. They also find a number of stars with $V - I > \sim 4$. We find no such stars in our proper motions selected sample. The reason for this could either be that the stars are saturated in our *I*-band images or that they happen to be outside our field of view. We are not in a position to be able to further distinguish between these possibilities.

8. The age of NGC 6528

Armed with the cleanest colour-magnitude diagram so far for the globular cluster NGC 6528 we are in a position to address its age using both stellar isochrones as well as in relation to other well studied metal-rich globular clusters.

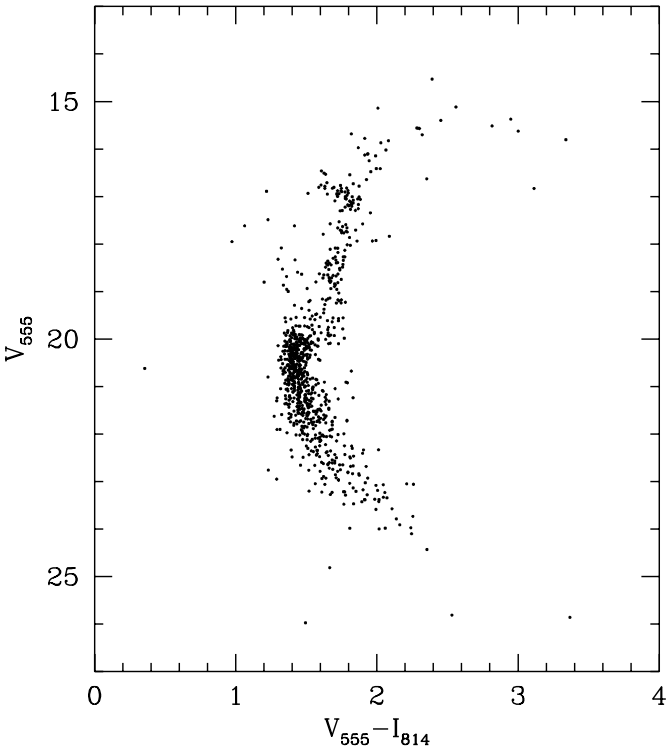

Fig. 15. Final colour-magnitude diagram based on the data from WF2 and WF3 corrected for differential reddening. Cuts in $\sqrt{\mu_l^2+\mu_b^2}$ as in Fig. 7.

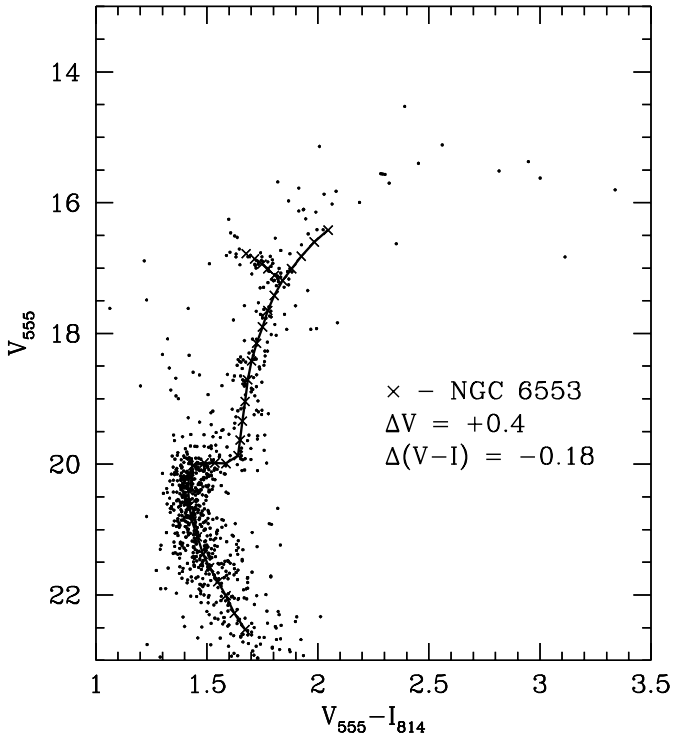

Fig. 16. Comparison of our final colour-magnitude diagram with the ridge line derived for NGC 6553 by Zoccali et al. (2001). Their ridge line is showed as a set of connected × symbols. Both the mains-sequence, red giant branch as well as the horizontal branch coincide well. The ridge line of NGC 6553 was moved +0.4 mag in V_{555} and −0.18 in $V_{555}-I_{814}$.

8.1. The metallicity of NGC 6528

Since age and metallicity are degenerate in colour-magnitude diagrams it is important to have a good estimate of the metallicity if we want to use stellar isochrones to find the absolute age of the cluster. In Table 1, we summarize the current metallicity and iron abundance estimates for NGC 6528 available in the literature.

Due to the faintness of metal-rich globular clusters detailed stellar abundance studies of individual stars in these clusters have been few. The results of the first such study was reported in Barbuy (1999) who obtained spectra of one, very cool ($T_{\rm eff}$ = 3600 K) giant star in NGC 6528 and derived a [Fe/H] of −0.6 dex, [Ca/Fe] = 0.0 dex and [Ti/Fe] = +0.6 dex.

Using the HIRES spectrograph on KECK Carretta et al. (2001) and Cohen et al. (1999), in two accompanying papers, derive iron abundances as well as abundances for a large number of other elements for four stars in NGC 6528 and five stars in NGC 6553. Carretta et al. (2001) found that all four stars in NGC 6528 show very similar [Fe/H] (+0.05, +0.08, +0.09, +0.04 dex respectively) thus their final [Fe/H] estimate for the whole cluster appears very robust. The accompanying study of NGC 6553 and the discussion of the [Fe/H] for NGC 6553 appear to indicate that a total error in [Fe/H] on the order of 0.1 dex appear a reasonable estimate (see detailed discussions in Carretta et al. 2001).

See also their detailed discussion of the problems with analysis of cold giants. It appears that the disagreement between the two studies could be due to different temperature scales having been used. Since the Carretta et al. (2001) study is the larger one and also guided by their discussion on the temperature and errors from other sources we here give higher weight to that study for determination of stellar abundances in NGC 6528. However, further independent studies of the stellar abundances in this cluster should be undertaken to solve this issue.

Further Carretta et al. (2001) found that the α-elements Si and Ca in NGC 6528 show large excesses compared to the solar values, while Ti and Mg appear to be solar. This type of abundance pattern is reminiscent of that observed for stars in the Galactic bulge (McWilliam & Rich 1994) and might be indicative of a rapid chemical enrichment process prior to the formation of the stars observed. The exact interpretation of these data is, however, pending.

In Carretta et al. (2001) the cluster membership for the four stars studied was ascertained by observing only horizontal branch stars. The stellar spectra were also used to derive radial velocities for the program stars and their velocities further confirmed the cluster membership for the four targets.

Having assessed the currently available abundance information for NGC 6528 we find it safe to assume that the cluster is probably as metal-rich as the sun and is enhanced, at least in some, $\alpha-$elements.

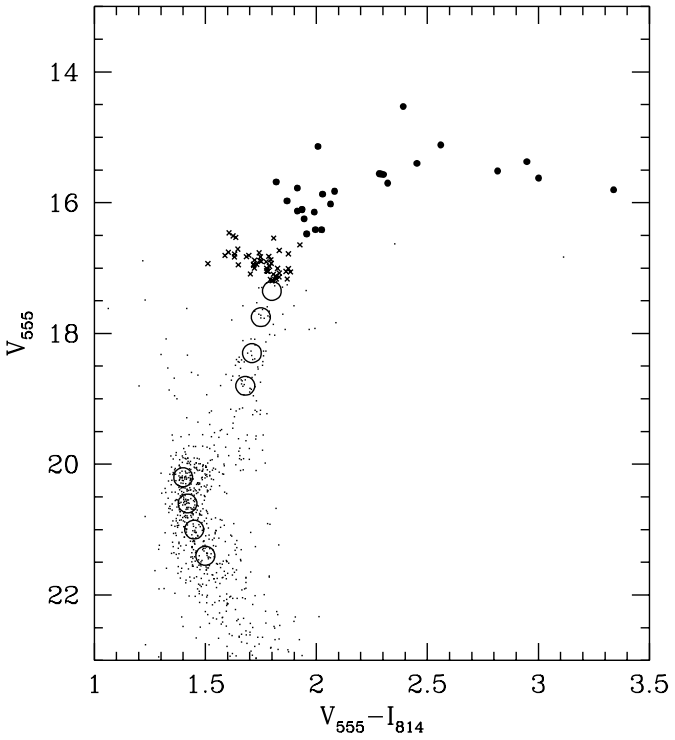

Fig. 17. Colour-magnitude diagram with fiducial points indicated by large open circles. The horizontal branch stars are indicated by × and the AGB stars with •. Note that no points are defined for the lower part of the red giant branch, see text for a discussion of this. Cuts in $\sqrt{\mu_l^2 + \mu_b^2}$ as in previous plots.

8.2. Comparison with NGC 6553

In Fig. 16 we compare the ridge line for NGC 6553 found by Zoccali et al. (2001) with our colour-magnitude diagram. To fit the colour-magnitude diagram for NGC 6528 with the ridge line of NGC 6553 we need to move the ridge line from Zoccali et al. (2001) by 0.4 in V_{555} and -0.18 in $V_{555} - I_{814}$. If the two clusters have the same metallicity (as indicated by the recent detailed abundance analyses) this nice fit indicates that their ages are very close too. We thus find that NGC 6553 has been more reddened than NGC 6528, i.e. the negative shift applied in $V_{555} - I_{814}$. Using Table 12 in Holtzman et al. (1995b) we find that shift in $V_{555} - I_{814}$ corresponds to a shift in V_{555} of -0.46. Thus NGC 6553 appears to be marginally closer to us that NGC 6528. However, it should be remembered that both in Zoccali et al. (2001) and in this work the colour-magnitude diagrams have been corrected for differential reddening so the interpretation of such shifts is less clear in terms of distance modulus. The $\Delta E(B-V)$, as measured here, between the two clusters is $\sim$0.15, using Table 12 in Holtzman et al. (1995b).

The agreement between the NGC 6553 ridge line and our data is very good. At the brightest end the NGC 6553 ridge line appears to fall slightly below the NGC 6528 data. However, since the NGC 6553 data does not go as bright as the NGC 6528 data one should not draw any conclusions regarding the relative metallicities of the clusters from this.

This comparison does, as has also been reported in e.g. Ortolani et al. (1995), show that these two clusters have indeed very similar ages.

Table 8. Fiducial points for NGC 6528.

$V_{555} - I_{814}$	V_{555}
1.5	21.4
1.45	21
1.42	20.6
1.4	20.2
1.68	18.8
1.71	18.3
1.75	17.75
1.8	17.35

8.3. Age from fitting stellar isochrones

Since NGC 6528 is found to be enhanced, at least in some, $\alpha-$elements we compare our fiducial points with that of theoretical stellar isochrones from Salasnich et al. (2000) in which α-enhancement has been included. To facilitate the comparison with the stellar isochrones we define a set of fiducial points which are shown in Fig. 17 and tabulated in Table 8.

The fiducial points are marked with large circles and trace the upper main-sequence as well as the upper part of the red giant branch. We have deliberately not defined any point for the lower red giant branch or for the sub-giant branch as we feel that these regions are less well defined and thus that any fiducial point might be misleading. We have also marked those stars that we will explicitly show in the diagrams where we fit isochrones. It is fairer to show all the AGB and horizontal branch stars rather than try to represent them with a fiducial line since then each reader is able to judge for themselves the goodness of the fit.

Examples of fits are shown in Fig. 18.

In the case of $Z = 0.019$ we moved the isochrones by $\Delta(V_{555}) = 15.95$ and $\Delta(V_{555} - I_{814}) = +0.63$. The turn-off is well represented by the 11 Gyr isochrone and the horizontal branch is well matched too. However, all the isochrones are brighter than the AGB. In order for $Z = 0.019$ isochrones to fit our data on the AGB we would need to increase the distance modulus and the best fitting isochrone would then be very young, younger than 9 Gyr. The horizontal branch would not be well fitted either. Thus it appears unlikely that our data could be well fitted with α-enhanced isochrones with $Z = 0.019$.

For the $Z = 0.040$ isochrones we moved them with the following amount $\Delta(V_{555}) = 15.95$ and $\Delta(V_{555} - I_{814}) = +0.655$. Here the AGB is much better reproduced and both turn-off and horizontal branch can be well fitted simultaneously. The 11 Gyr isochrone appears to fit best.

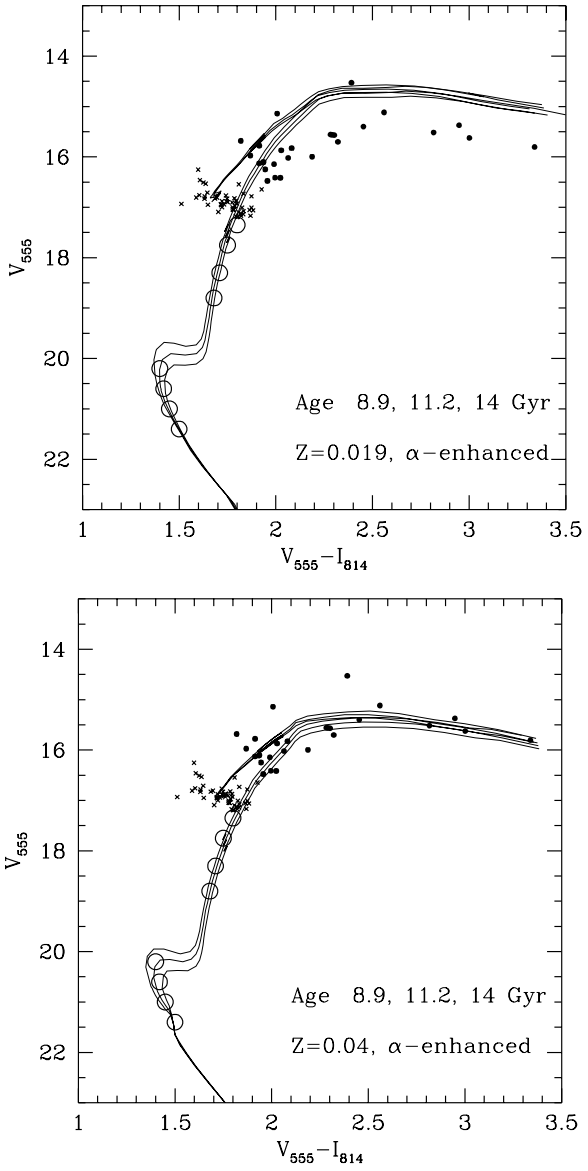

Fig. 18. Fiducial points for NGC 6528 together with stellar isochrones from Salasnich et al. (2000). Isochrones are for $Z = 0.019$ and $Z = 0.040$. Horizontal branch stars and AGB stars are coded as previously.

However as this fit cannot be rigorous due to the limitations in the data the estimated error bar on this must be rather large, perhaps up to 2 Gyr.

These ΔV_{555} and $\Delta(V_{555} - I_{814})$ correspond to (using Table 12 in Holtzman et al. 1995a) an $E(B-V)$ of 0.54 and thus a distance modulus of 14.29 which corresponds to a physical distance of 7.2 kpc. The derived distance, is compatible with that found by Richtler et al. (1998) who used the magnitude of the horizontal branch to determine the distance to NGC 65628. With $m_v(\mathrm{HB}) = 17.21 \pm 0.05$ they found that the distance to NGC 6528 is between 6.0 and 8.9 kpc depending on the exact value for reddening and metallicity as well as the relation between magnitude for the horizontal branch and metallicity (see their Table 10). Since we have a better handle on the metallicity we are able to be more sure about the distance and reddening. Note that the reddening that we derive here is a "minimum" reddening in the sense that we have dereddened the stars on WF3 relative to those on WF2 according to the differential reddenings found.

9. Discussion and summary

Colour-magnitude diagrams of the metal-rich globular cluster NGC 6528 are notoriously difficult to analyze. This is due to the fact the cluster is situated in the Galactic bulge and thus the fields stars belonging to the bulge have the same magnitudes as the stars in NGC 6528.

Using two epochs of observations with HST/WFPC2 we obtain the stellar proper motions for all stars in the field. The proper motions are used to separate the bulge from the cluster stars. The stellar sequences in the resulting colour-magnitude diagram are better defined than in any previously published colour-magnitude diagram.

Using α-enhanced stellar isochrones we find NGC 6528 to have a probable age of 11 ± 2 Gyrs, this is the first attempt to establish the absolute age of NGC 6528. Previous studies have only compared the fiducial ridge line for the cluster to that of other globular clusters of similar metallicities. Mainly the comparisons have been with regards to NGC 6553 and 47 Tuc. With the new metallicity determinations for individual stars in both NGC 6553 and NGC 6528 it is now clear that 47 Tuc (at -0.71 dex) has a significantly lower metallicity than NGC 6528 and NGC 6553 and is thus not a suitable comparison cluster as regards differential age determinations (see e.g. Stetson et al. 1996 and references therein).

The distance modulus obtained when fitting the stellar isochrones yields a distance to NGC 6528 of 7.2 kpc, fully compatible with previous derivations.

A comparison with the fiducial line for NGC 6553 confirms results in earlier studies, e.g. Ortolani et al. (1995), that the two clusters indeed have very similar ages.

The stellar proper motion also provide velocity dispersions for both the cluster and field stars. The velocity dispersion of the cluster is most likely dominated by measurement errors. The bulge dispersion can thus be found by deconvolution. The resulting dispersions are consistent with what has previously (Spaenhauer et al. 1992) been found for Bulge giants. Moreover, combining our results with those by Zoccali et al. (2001) we are able to confirm the difference in σ_l at two positions in the bulge as predicted by the model in Zhao (1996).

To our knowledge, our and Zoccali et al.'s study are the first to address the proper motions amongst bulge horizontal branch and fainter stars.

Finally we derive the mean proper motion of NGC 6528 relative to the Galactic bulge and also the space velocities. We find $< \mu_l > = \sim +0.006$ and $< \mu_b > = \sim +0.044$ arcsec per century and $(\Pi, \Theta, W) = (-142, 303, 4)$ km s^{-1}.

Acknowledgements. We thank the Royal Swedish Academy of Sciences for a collaborative grant that enabled visits to Cambridge, for SF, and to Lund, for RAJ.

Appendix A: Stellar proper motions, coordinates and magnitudes

Table A.1. Stellar proper motions, both in galactic coordinates as well as in position on WF2-chip. The proper motions in galactic coordinates are given in arcsec per century. Magnitudes and errors on magnitudes are also given. The table contains data for all stars brighter than $V_{555} = 19$ and which did not have fitting errors. The position on the WF chip are for the new images. The full table (containing 212 entries) is available electronically from CDS.

μ_l	μ_b	l	b	Δx	Δy	x	y	V_{555}	σ_{V555}	I_{814}	σ_{I814}
–0.134	–0.326	1.142	–4.155	–0.350	–0.038	614.45	42.80	17.18	0.001	15.33	0.003
0.162	0.038	1.139	–4.169	0.082	0.145	120.38	48.03	17.15	0.002	15.41	0.003
–0.265	–0.065	1.140	–4.164	–0.136	–0.237	296.42	48.49	17.35	0.002	16.00	0.004
0.069	0.023	1.139	–4.167	0.041	0.060	179.20	54.49	16.95	0.001	15.30	0.003
...	...	...	...	...	...	...	...	...	...	...	...
...	...	...	...	...	...	...	...	...	...	...	...
...	...	...	...	...	...	...	...	...	...	...	...

Table A.2. Stellar proper motions, both in galactic coordinates as well as in position on WF3-chip. The proper motions in galactic coordinates are given in arcsec per century. Magnitudes and errors on magnitudes are also given. The table contains data for all stars brighter than $V_{555} = 19$ and which did not have fitting errors. The position on the WF chip are for the new images. The full table (containing 214 entries) is available electronically from CDS.

μ_l	μ_b	l	b	Δx	Δy	x	y	V_{555}	σ_{V555}	I_{814}	σ_{I814}
–0.207	–0.077	1.146	–4.173	–0.177	0.132	354.99	61.06	18.64	0.005	17.14	0.009
0.102	–0.039	1.145	–4.173	0.109	0.009	327.54	74.75	18.80	0.004	17.15	0.007
–0.080	–0.076	1.145	–4.173	–0.055	0.095	340.09	76.76	16.99	0.001	15.27	0.003
0.024	–0.101	1.147	–4.175	0.051	0.090	398.59	101.47	17.00	0.001	15.29	0.003
...	...	...	...	...	...	...	...	...	...	...	...
...	...	...	...	...	...	...	...	...	...	...	...
...	...	...	...	...	...	...	...	...	...	...	...

Table A.3. Stellar proper motions, both in galactic coordinates as well as in position on WF4-chip. The proper motions in galactic coordinates are given in arcsec per century. Magnitudes and errors on magnitudes are also given. The table contains data for all stars brighter than $V_{555} = 19$ and which did not have fitting errors. The position on the WF chip are for the new images. The full table (containing 227 entries) is available electronically from CDS.

μ_l	μ_b	l	b	Δx	Δy	x	y	V_{555}	σ_{V555}	I_{814}	σ_{I814}
0.528	0.055	1.136	–4.175	–0.205	–0.490	217.89	51.06	17.29	0.005	15.51	0.006
–0.032	0.045	1.136	–4.175	–0.034	0.044	216.26	55.69	17.23	0.005	15.46	0.005
–0.186	0.115	1.135	–4.177	–0.056	0.211	292.08	55.84	18.81	0.009	17.25	0.017
0.868	–0.076	1.137	–4.172	–0.178	–0.853	88.79	57.58	17.35	0.004	15.52	0.005
...	...	...	...	...	...	...	...	...	...	...	...
...	...	...	...	...	...	...	...	...	...	...	...
...	...	...	...	...	...	...	...	...	...	...	...

References

Armandroff, T. E., & Zinn, R. 1988, AJ, 96, 92

Arp, H. 1986, A&A, 156, 207

Baggett, S., Casertano, S., Gonzaga, S., & Ritchie, C. 1997, WFPC2 Instrument Science Report 97-10

Barbuy, B. 1999, in Galaxy Evolution: Connecting the Distant Universe with the Local Fossil Record, ed. M. Spite, 319

Bedin, L. R., Anderson, J., King, I. R., & Piotto, G. 2001, ApJ, 560, L75

Bica, E. L. D., & Pastoriza, M. G. 1983, Ap&SS, 91, 99

Bruzual, G., Barbuy, B., Ortolani, S., Bica, E. Cuisinier, et al. 1997, AJ, 114, 1531

Carretta, E., Cohen, J.G., Gratton, R.F., & Behr, B.B. 2001, AJ, 122, 1469

Cohen, J. G., & Sleeper, C. 1995, AJ, 109, 242

Cohen, J. G., Gratton, R. G., Behr, B. B., & Carretta, E. 1999 ApJ, 523, 739
Cudworth, K. M. 1988 AJ, 96, 105
Davidge, T. J. 2000, ApJS, 126, 105
Dehnen, W., & Binney, J. J. 1998, MNRAS, 298, 387
Dubath, P., & Grillmair, C. J. 1997, A&A, 321, 379
Dubath, P., Meylan, G., & Mayor, M. 1997, A&A, 324, 505
Feltzing, S., & Gilmore, G. 2000, A&A, 355, 949
Ferraro, F. R., Messineo, M., Fusi Pecci, F., De Palo, M. A., Straniero, O., et al. 1999, AJ, 118, 1738
Fruchter, A. S., & Mutchler, M. 1998, STScI preprint (avialable from `www-int.stsci.edu/fruchter/dither/ditherII.ps`)
Gonzaga, S., O'Dea C., & Whitmore, B. 1999, WFPC2 Technical Instrument Report 99-01
Harris, W. E. 1996, AJ, 112, 1487
Heitsch, F., & Richtler, T. 1999, A&A, 347, 455
Holtzman, J., Hester, J. J., Casertano, S., & Trauger, J. T., Watson, A. M. 1995a, PASP, 107, 156
Holtzman, J. A., Burrows, J., Casertano, S., Hester, J. J., Trauger, J. T. 1995b, PASP, 107, 1065
Holtzman, J. A., Watson, A. M., Baum, W. A., Grillmair, C. J., Groth, E. J., et al. 1998, AJ, 115, 1946
King, I. R., Anderson, J., Cool, A. M., & Piotto, G. 1998, ApJ, 429, L37
McWilliam, A., & Rich, M. 1994, ApJS, 91, 749
Origlia, L., Ferraro, F. R., Fusi Pecci, F., & Oliva, E. 1997, A&A, 321, 859
Ortolani, S., Barbuy, B., & Bica, E. 1991, A&A, 249, 310
Ortolani, S., Bica, E., & Barbuy, B. 1992, A&AS, 92, 441
Ortolani, S., Renzini, A., Gilmozzi, R., et al. 1995, Nature, 377, 701
Pryor, C., & Meylan, G. 1993, in Structure and Dynamics of Globular Clusters, ed. S. G. Djorgovski & G. Meylan, ASP Conf. Ser., 50, 357
Richtler, T., Grebel, E. K., Subramaniam, A., & Sagar, R. 1998 A&AS, 127, 167
Sadler, E. M., Rich, R. M., & Terndrup, D. M. 1996, AJ, 112, 171
Salasnich, B., Girardi, L., Weiss, A., & Chiosi, C. 2000, A&A, 361, 1023
Spaenhauer, A., Jones, B. F., & Whitford, A. E. 1992, AJ, 103, 297
Stetson, P. B., VandenBerg, D. A., & Bolte, M. 1996, PASP, 108, 560
Whitmore, B., Heyer, I., & Casertano, S. 1999, PASP, 111, 1559
Zhao, H. S. 1996, MNRAS, 283, 149
Zinn, R. 1980, ApJS, 42, 19
Zinn R., & West, M. 1984, ApJS, 55, 45
Zoccali, M., Renzini, A., Ortolani, S., Bica, E., & Barbuy, B. 2001, AJ, 121, 2638